Interferometric Gravitational Wave Detection

François Bondu

Interferometric gravitational wave detection*

F. Bondu
ARTEMIS, CNRS, Observatoire de la Côte d'Azur
BP 4229 06304 Nice CEDEX 4, France
bondu@oca.eu

Abstract

Gravitational waves are deformations of space-time. The beating of the local clock of an inertial observer with the time given by photons travelling between two points is sensitive to these waves. Actual instruments consists in Michelson interferometers with Fabry-Perot cavities in the arms. The thermal noise of the mirror suspensions and of the mirror bulks limit the spectral density of the resolution in the 10 Hz - 200 Hz range; the detected shot noise is the resolution limit in the 200 Hz - 10 kHz range. We give the status of actual interferometers. Advanced detectors, in operation in the next decade, open new technical challenges.

*This series of lectures was delivered at Ecole Prédoctorale des Houches, session XXIV, Quantum Optics, September 10-21, 2007. The session was directed by Nicolas Treps and Isabelle Robert-Philip.

Contents

1 Principles of detection of gravitational waves

Astrophysical or cosmological events (supernovae collapses, final phases of the coalescence of two neutron stars, coalescences of two blak holes, rotating pulsars, cosmological or astrophysical background, etc.) emit gravitational waves. These are, on earth, plane waves that appear as a deviation to the flat space-time. If the z axis is the wave propagation direction, a space-time element $\mathrm{d}s^2$ writes [1]

$$\mathrm{d}s^2 = c^2\mathrm{d}t^2 - (1+h_+(t))\,\mathrm{d}x^2 - (1-h_+(t))\,\mathrm{d}y^2 - \mathrm{d}z^2 - 2\,h_\mathrm{x}(t)\,\mathrm{d}x\,\mathrm{d}y \quad (1)$$

where h_+ and h_x are the two polarizations of the tensorial gravitational wave and c is the speed of light in vacuum.

A clock at rest with coordinates $(0,0,0)$ measures the time for a photon to travel back and forth from the two points with coordinates $(0,0,0)$ and $(L,0,0)$. The one way propagation time is, using $\mathrm{d}s^2 = 0$, $\tau_{(x=L)} = \int_0^{\tau_{(x=L)}} \mathrm{d}t$. Using eq. (1) and using the approximation $|h(t)| \ll 1$ we obtain

$$\tau_{(x=L)} = \frac{L}{c} + \frac{1}{2}\int_0^{L/c} h_+(t)\,\mathrm{d}t\ . \quad (2)$$

When the wavelength of h_+ is much longer than L, then $\tau_{(x=L)} = \frac{L}{c}(1 + \frac{1}{2}h_+(t))$. The variation of the round trip travel time with respect to the expected $2L/c$ is then $h_+ L/c$; its relative variation is $h_+/2$.

We consider instruments able to detect gravitational waves in the 10 Hz - 10 kHz frequency band. We analyze the spectral content of the random signals using the power spectral density that is the Fourier transform of the auto-correlation function. The linear spectral density is the square root of the power spectral density. The systems considered are linear with respect to the linear spectral density.

The realization of sets of coordinates requires free-falling (inertial) test masses. We show here that suspended test masses achieve that goal above the pendulum frequency. The displacement response of the test mass with mass M to a force applied on the test mass is

$$\tilde{x}(f) = \tilde{F}(f)\frac{1}{M(2\pi)^2(f_0^2 - f^2 + if f_0/Q)} \tag{3}$$

so that a test mass suspended at a pendulum behaves as an inertial mass for frequencies above the pendulum frequency.

The pendulum also achieves isolation from seismic noise. The displacement response of a suspended test mass to the seismic noise applied on the pendulum suspension point is

$$\tilde{x}(f) = \tilde{x}_{\rm seism}(f)\frac{1}{1 - (\frac{f}{f_0})^2 + i\frac{f}{f_0 Q}} \tag{4}$$

where f_0 is the pendulum frequency and Q is the quality factor of the pendulum resonance. On ground, a pendulum achieves isolation from seismic noise for analysis frequencies above pendulum frequency.

The frequency of a laser realizes a clock. The two suspended mirrors of a Fabry-Perot cavity realize two sets of coordinates. We assume that the laser frequency is tuned so that the laser is resonant in the cavity. The laser beam is split in two parts. The first one resonates and realizes the photons travelling between the two sets of coordinates. The second part does not resonate and realizes the local clock. There are several ways to split a beam in order to have both resonant and non resonant beams, and to recover a signal proportional to the detuning:

- The laser is phase modulated at a frequency $f_{\rm m}$, where $f_{\rm m}$ is larger than the cavity linewidth [2, 3]. This is the technique used in actual interferometric gravitational wave detectors.

- The input laser beam is sligthly tilted with respect to the resonating beam; with respect to the cavity axis, the beam is then the sum of TEM00 and TEM01 modes. The cavity is designed so that the two modes do not resonate simulatneously [4].
- If the cavity contains a birefringent material, the input beam polarization decomposes on the two axes [5].
- Some of the light is diverted to a reference arm. This technique will be used in second generation interferometric gravitational wave detectors.

The extra phase between resonant and non resonant light is $2\pi\nu_0 L\, h_+(t)/c$ per round trip with respect to the situation where no gravitational wave is present.

A frequency noise verifying $\delta\nu = \nu_0 h(t)/2$ produces a similar extra phase: the relative frequency noise should be of the same order of magnitude than the resolution level for gravitational wave detection; this is not the case with a free-running laser. The actual gravitational wave detectors use a Michelson configuration, with two km-scale perpendicular Fabry-Perot cavities in the arms. The Michelson interferometer is tuned on the dark fringe, where the two signals proportional to h_+ from the Fabry-Perot cavities add up. The frequency noise cancels on that dark fringe down to an asymmetry factor of the order of 1 %. The frequency noise is stabilized on the common motion of the two Fabry-Perot arms, using the light reflected by the interferometer as described in fig. 1. The frequency noise forbids the detection of the h_{x} polarization or a scalar component of the gravitational wave using the light reflected by the interferometer.

2 Sensitivity and resolution

2.1 Sensitivity

The sensitivity of a Pound-Drever-Hall signal to a gravitational wave h is proportional to the laser power P_0 and inversely proportional to the cavity pole f_P:

$$s_{\mathrm{PDH}}(f) = K P_0 m (1+\zeta) \frac{\nu_0}{f_P} \frac{h}{2} \tag{5}$$

where K is the product of the photodiode gain, of the mixer loss factor and of the photodiode transimpedance; and the demodulation wave amplitude,

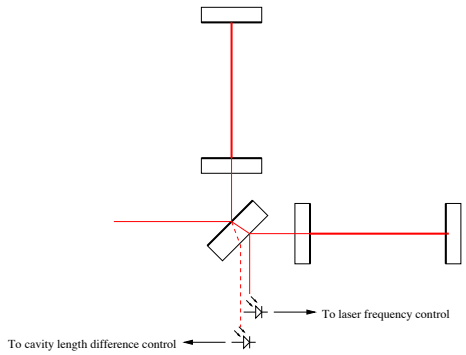

Figure 1: In a Michelson interferometer configuration, the dark fringe is the channel to look for gravitational waves whereas the frequency noise is measured on one of the bright fringes, either in the light reflected by the interferometer or on the light on the second face of the beam splitter.

$m \ll 1$ is the modulation index, ζ is the amplitude cavity reflectivity at resonance ($\zeta = 1$ for an over-coupled cavity) and ν_0 is the laser frequency. The cavity pole is the half linewidth of one resonance: $f_P = \frac{c}{4\mathcal{F}L}$, where $\mathcal{F}$ is the cavity finesse.

When the interferometer is tuned on the dark fringe, most of the light is reflected towards the laser. An additional mirror, the recycling mirror, provides an additional Fabry-Perot cavity that amplifies the effective laser power on the beam-splitter; the sensitivity increases proportionally to the build-up factor of the recycling cavity, see fig. 2. The losses $L_{\rm arm}$ in the long arms (a few hundreds ppm) limit the build-up factor and the finesse of the arms. The absorption and the non perfect surface figure of the mirrors (some of the light is scattered out of the cavity, some is converted in non resonating modes) cause these losses. The practical finesse $\mathcal{F}$ for the long arms varies from 50 (Virgo) to 220 (LIGO). The reflectivity defect of the arms is then $1 - R_{\rm arm} \sim L_{\rm arm} * 2\mathcal{F}/\pi$. The optimum intensity reflectivity factor for the recycling mirror would be $R_{\rm arm}$.

The difference of the two distances between the beam splitter and the cavity front mirrors is chosen such that a fraction of the sidebands is transmitted to the dark fringe. The modulation frequency is chosen such that the sum of the two sidebands resonates in the recycling cavity.

A full description of the gravitational wave effect on Fabry-Perot cavities, similar to the one done in eqs. 1-2, allows to compute the antenna pattern [6].

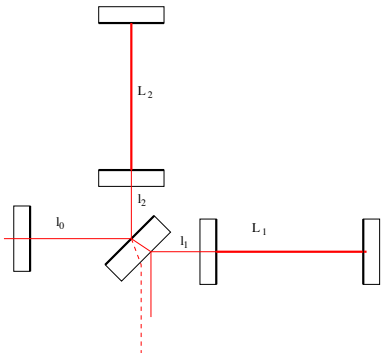

Figure 2: A Michelson interferometer with Fabry-Perot cavities in the arm and a power recycling mirror offers a good sensitivity compatible with the effective visibilities of the cavities.

The pattern of fig. 3 is valid for all analysis frequencies small with respect to the first free spectral range of the long arms (50 kHz).

A single antenna has little angular resolution on the sky. The analysis of the arrival time delays from the network of LIGO (U.S.A) and Virgo (France-Italy) antennas, well spread on the earth surface, allows to reconstruct the direction of an incoming wave.

2.2 Resolution from fundamental noises

The realization of coordinates with real test masses can not be achieved with an infinite resolution. The mirrors and their suspensions are thermally at equilibrium with their environment. Each degree of freedom (pendulum resonance, modes of the mirror) is excited by a Langevin's force $\frac{1}{2}k_BT$. According to the fluctuation-dissipation theorem, there is a residual motion of the mirror surface [7]:

$$|\tilde{x}^2(f)| = \frac{4k_BT}{2\pi f}\mathrm{Im}\left(\frac{1}{\chi}\right) \tag{6}$$

where χ is the transfer function from a force to a displacement (see eq. 4).

The laser beam scans the surface, averaging the displacement with the mode shape. This results in an effective mass for each mode, and the apparent

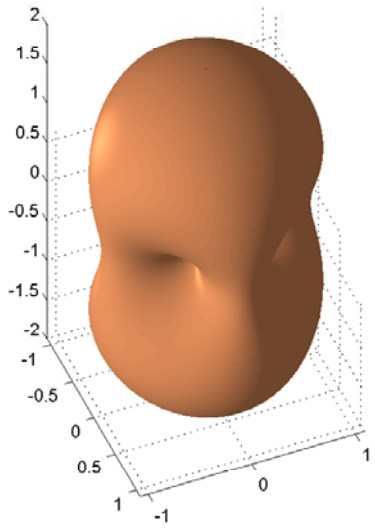

Figure 3: Antenna pattern of the Michelson interferometer. The inteferometer arms are oriented along x and y axes.

displacement of the test mass is:

$$|\tilde{x}^2(f)| = \frac{4k_BT}{(2\pi)^3} \sum_n \frac{\phi(f) f_n^2}{M_n f \left[f_n^4 \phi^2(f) + (f_n^2 - f^2)^2\right]} \tag{7}$$

where the sum is on all resonant modes : pendulum mode, violin modes of the suspensions, internal vibrations of the mirrors. ϕ is the loss angle of acoustic waves. We assume internal damping of acoustic waves in this formula, rather than a viscous damping.

The displacement effect on the spectral resolution is divided by the arm length; km-scale cavities is the solution to reduce the thermal noise effect in the spectral density of the resolution.

The clock is realized with photons; the quantum nature of photons forbids the realization of the clock with an infinite precision. We assume a semi-classical model where the arrival times of photons are distributed with a Poisson law; then the standard deviation for counting N photons during a period ΔT is $\sqrt{N}$.

In real interferometers, the dark fringe power is dominated by high order modes caused by the optical defects of mirror surfaces. As this light would

only contribute to the noise and not to the signal, an output mode cleaner cavity filters out the high order modes.

The sidebands, that are not stationary, dominate the shot noise in the dark fringe, after the mode filtering. A calculation leads to a spectral resolution of [8]

$$\tilde{h}(f) = \frac{f_{\rm p}}{\nu_0}\sqrt{\frac{h\nu}{2P_0}}\frac{\sqrt{G(1-C)+1.5m^2T}}{m\sqrt{GT}}\sqrt{1+\left(\frac{f}{f_{\rm p}}\right)^2} \qquad (8)$$

where the signal to noise ratio for the resolution is set to 1; $f_{\rm p}$ is the pole of the km-scale Fabry-Perot cavities, ν_0 the laser frequency, $1-C$ the contrast defect of the Michelson interferometer for the carrier, T the transmission of the sidebands and G the power build-up factor in the recycling cavity.

2.3 Resolution from technical noises

There are various noise sources that might limit the resolution if no careful design is achieved.

Four longitudinal degrees of freedom control the recycled interferometer. Unfortunately, the sensing and control matrix are not diagonal. Digital filters modify the control filters to substract these spurious effects, and the resolution improves by a factor 100 in the 10 Hz - 150 Hz frequency band.

The micro-roughness of the mirrors scatters a few ppm of the light that resonates in the long arms; this light is scattered on the vacuum tubes, and may recombine into the main beam after an additional phase noise due to the seismic motion of vacuum pipes. A set of baffles in the vacuum tubes is designed to reduce the recombining scattered light to negligible levels [9].

The laser power noise may couple with beam misalignments to produce spurious signals. A cavity with suspended mirrors, the input mode-cleaner, filters out the laser beam pointing jitter. A servo loop controls the power transmitted by this cavity.

2.4 Data analysis

The performance of one detector or a set of detectors is assesed with a false alarm rate at a given signal to noise ratio. If the waveform is well known, as for the final spirals before the coalescence of two neutron stars, a matched filter helps to recover some signal to noise ratio.

3 Detectors and status

There are four kilometer scale detectors: Virgo, in Pisa, Italy, from a French-Italian collaboration, is an interferometer with 3 km arms [11]. LIGO (MIT/Caltech) is a set of three detectors [12], two collocated in Washington state (4 km and 2 km arms) and one in Louisiana state (4 km arms). GEO is an interferometer with 600 m folded arms, without Fabry-perot cavities, set in Hanover (Germany) [13]. TAMA is a Japanese interferometer with 300 m arms sensitive enough to see events in the galaxy [14]. ACIGA is an Australian prototype to test high powers in interferometers [15].

LIGO is taking data with the design spectral resolution for the first generation since December 2005. The instruments are able to see the final spirals before the coalescence of two 1.4 solar mass neutron stars at a distance of 15 Mpc, averaged on polarizations and antenna pattern. Virgo is able to see that same signal with an horizon of 3.5-4 Mpc. A common data taking of LIGO, GEO and Virgo instruments has started in May 2007 [16].

4 Advanced detectors and challenges

The current detectors will be upgraded in 2008, leading to the 1.5 generation. This consists mainly in increasing the laser power from 20 to 50 W, improving the seismic isolation, increasing the finesse of the long arms.

In 2020, the second generation of interferometers would be ready. The laser power will be increased up to 200 W; the thermal noise of test masses will be improved; the optical losses will be reduced enough to increase the finesse to about 800.

In 2030, the third generation will include large beam profiles and cryogenic masses.

4.1 Resolution from fundamental noises

The dissipation of acoustic waves in the mirror bulk and coating is the cause of the thermal motion of the mirror surfaces. The main dissipation occurs in the high index layers of the coating. R&D is going on to reduce this contribution to the spectral resolution: the lines are reduction of the dissipation factor with proper design of the material of the high index layers, and alternative design of the layers.

Large beams would better average the surface deformation from thermal noise. Flat-top beams, high order Laguerre-Gauss modes, or fiber LP modes would reduce the thermal noise by a factor of 3-4.

The cooling of the mirror to cryogenic temperatures could be the ultimate solution for third generation interferometers, as designed for the LCGT Japanese project. The gain is not only on the temperature factor, but on the quality factor of resonances as well.

A higher laser power entering the interferometers decreases the shot noise level. Second generation interferometers will have an input power of 200 W.

The suppression of the sidebands on the dark fringe reduces the shot noise level. A small offset on the dark fringe will substract the two carrier signals from the two Fabry-Perot cavities. This technique is known as DC detection.

A mirror placed on the dark port of the interferometer can make a Fabry-Perot cavity where the signal would be recycled, not the carrier. This technique is known as signal recycling and resonant sideband extraction [17].

The radiation pressure noise will limit the spectral resolution in second generation interferometers, in the low frequency region. The introduction of a squeezed vacuum in interferometers would decrease the noise below the quantum limit resulting from the shot-noise and the radiation pressure noise [18], depending on the effective losses in the interferometer. The squeezing angle between phase and amplitude would need to be frequency dependent.

4.2 Resolution from technical noises

The absorption of light in the mirror bulks and coatings deforms the mirror surface and produces a lens since the SiO2 index is sensitive to temperature. The design of thermal compensation systems, with CO2 lasers illuminating the mirror surfaces, ensures nominal beam parameters and beam wavefront matching. This system helps to ensure a stable recycling cavity for the sidebands. Large beams (high order Laguerre-Gauss modes, flat top modes) will also reduce the mirror lens in the second generation interferometers.

If the laser power is large enough in the Fabry-Perot cavities, parametric instabilities can occur. The condition is, for a given mirror vibration frequency, that the excited spatial mode can resonate [19]: the spatial mode frequency detuning from fundamental mode fits within the cavity linewidth with the mirror mode resonance frequency, and the mirror surface deformation matches the excited mode wavefront. The mitigation of the effect might

involve the damping of mirror modes without degradation of the thermal noise read by the main beam.

The mirrors of interferometric detectors are dielectric masses placed in vacuum. Cosmic rays or other sources charge them with time, so that the test masses become sensitive to static electrical and magnetic fields. The effect level is under investigation.

5 Conclusion

The km-scale interferometers realize the measurement of the travel time of photons in a wavy space time. First generation detectors are ready. A detection rate of a few gravitational wave events per day requires the design of advanced instruments. These observatories will probably be ready in the next decade. This opens exciting technical challenges in metrology.

References

[1] É. Gourgoulhon, *Cours de relativité générale, master, http://www.luth.obspm.fr/ luthier/gourgoulhon/fr/master/relatM2.pdf*, (2006).

[2] R.V. Pound, *Rev. Sci. Instrum.***17**(1946) 490

[3] R.W.P. Drever, J.L. Hall, F.V. Kowalski, J. Hough, G.M. Ford, A.J. Munley and H. Ward, *Appl. Phys. B***31**(1983) 97

[4] M.B. Gray, D.A. Shaddock and D.E. McClelland, *Opt. Lett.***24**(1999) 1499

[5] T.W. Hänsch and B. Couillaud, *Opt. Commun.* **35** (1980) 441

[6] The Virgo Collaboration, *http://wwwcascina.virgo.infn.it/vpb/* 2006

[7] H.B. Callen and T.A. Welton, *Phys. Rev.***83**(1951) 34

[8] The virgo collaboration, *Appl. Opt.***46**2007 3466

[9] J.-Y. Vinet, V. Brisson, S. Braccini, I. Ferrante, L. Pinard, F. Bondu and É. Tournié, *Phys. Rev. D***56**(1997) 6085

[10] M. Smith, *http://www.ligo.caltech.edu/docs/G/G000008-00.pdf* (2000)

[11] Acernese F. et al., *Class. Quantum Grav.***23**(2007) S635

[12] S.J. Waldman et al., *Class. Quantum Grav.***23**(2006) S653

[13] S. Hild, *Class. Quantum Grav.***23**(2006) S643

[14] T. Akutsu, M. Ando, N. Kanda, D. Tatsumi, S. Telada, S. Miyoki, M. Ohashi et al., *Class. Quantum Grav.***23**(2006) S715

[15] P.J. Barriga et al., *Proc. SPIE 5500***70**(2004)

[16] CNRS, *http://www2.cnrs.fr/sites/en/fichier/dossier_ de_ presse_ en_ anglais.pdf* 2007

[17] P.R. Saulson, *Fundamentals of interferometric gravitational wave detectors, Ed. World Scientific* (1994)

[18] H. Vahlbruch, S. Chelkowski, B. Hage, A. Franzen, K. Danzmann and R. Schnabel, *Phys. Rev. Lett.***97**(2006) 011101

[19] C. Zhao, L. Ju, J. Degallaix, S. Gras and D. G. Blair, *Phys. Rev. Let.***94**2005 121102